Buried-interfacial reactivity of palladium-coated Fe_2O_3/FeTi thin films during vacuum or hydrogen annealing

1990 J. Phys.: Condens. Matter 2 5809

(http://iopscience.iop.org/0953-8984/2/26/018)

J. Phys.: Condens. Matter **2** (1990) 5809–5818. Printed in the UK

Buried-interfacial reactivity of palladium-coated Fe_2O_3/FeTi thin films during vacuum or hydrogen annealing

J H Sanders and B J Tatarchuk
Department of Chemical Engineering, Auburn University, Auburn, AL 36849, USA

Received 2 January 1990, in final form 9 March 1990

Abstract. FeTi is considered a good material for solid state hydrogen storage; however, it must undergo an initial activation by either a vacuum or hydrogen annealing procedure after preparation or exposure to air. Previous studies indicate that the initial activation in vacuum causes a reduction of surface iron oxides by a solid state reaction with FeTi to produce TiO_2. Palladium has also been shown to be an effective barrier for eliminating O_2 or H_2O impurities in typical H_2 charging gases from reaching active FeTi. These impurities cause FeTi decomposition to iron and TiO_2. In this study, experiments have been performed to investigate interfacial reactions that occur between Fe_2O_3 and FeTi layers located below protective palladium overlayers. Vacuum annealing procedures were found to crack the palladium overlayer while forming both iron and titanium oxides below the surface. Hydrogen annealing procedures allowed reduction of the subsurface Fe_2O_3 by FeTi without evidence of cracking within the palladium overlayer. Both procedures produced Fe–Pd alloys, the latter procedure also forming Fe–Pd hydrides at $\geq$623 K. Results indicate that the application of palladium overlayers on FeTi may be successfully used provided the initial activation is performed in hydrogen environments.

1. Introduction

FeTi has been shown to be a good material for the reversible solid state storage of hydrogen [1–3]. This material can accommodate 37% more hydrogen per unit volume than liquid hydrogen [4] and can be charged and discharged at reasonable temperatures and pressures. Reilly and Wiswall [1] produced pressure–composition isotherms for the FeTi–H system at temperatures from 273 to 343 K and over a pressure range from 10 to 10 000 kPa.

Problems encountered when using FeTi for hydrogen storage include: (i) an *initial activation* procedure is required after preparation or after exposure to air [5], and (ii) a gradual loss of efficiency, namely *cyclic deactivation* is experienced after a number of charge–discharge cycles [6]. Previous studies in our laboratory have addressed these problems using backscatter conversion electron Mössbauer spectroscopy (CEMS) and x-ray photoelectron spectroscopy (XPS) [7, 8]. Results indicated that initial activation procedures reduced surface iron oxides to metallic iron crystallites, which were capable of H_2 dissociation thereby assisting hydrogen incorporation into the FeTi bulk. It was noted that iron oxide reduction could occur from a solid state reaction with bulk FeTi as well as from direct reduction by gaseous H_2. Cyclic deactivation, on the other hand, was determined to occur from preferential reaction of titanium, in FeTi, with ppm levels

0953-8984/90/265809 + 10 $03.50

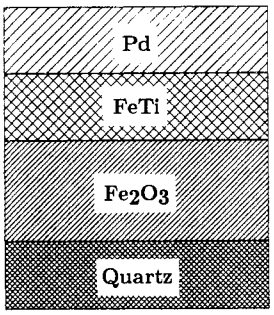

Specimen	Layer Thickness (nm)		
	Fe in Fe_2O_3	FeTi	Pd
1 - Vacuum	12.5	9.4	10.0
2 - Hydrogen	10.0	7.5	8.0

Figure 1. Specimen preparation for samples used in vacuum and hydrogen annealing procedures.

of O_2 and/or H_2O in the hydrogen-rich charging gas to produce TiO_2 and metallic iron. TiO_2 and iron are inert for hydrogen storage and progressively accumulated on the surface. The use of a palladium coating was found to effectively eliminate surface decomposition by acting as a barrier to O_2 and/or H_2O impurities thereby eliminating their contact with the underlying FeTi.

The study presented in this paper serves to clarify the reaction mechanisms of iron oxide reduction by adjacent FeTi during both vacuum annealing and hydrogen annealing processes. Both processes can be used to promote the initial activation of FeTi [9, 1]. The influence of O_2 and/or H_2O impurities is removed by the use of thin palladium overlayers. CEMS has been used extensively since it provides information about *subsurface* interfacial reactivity not readily obtained by other means.

2. Experimental details

2.1. Sample preparation

Specimens were prepared as shown in figure 1. Stoichiometric and equivalent layer thicknesses were determined according to the reaction

$$\tfrac{3}{4}FeTi + Fe_2O_3 \rightarrow \tfrac{3}{4}TiO_2 + \tfrac{7}{4}Fe^0 + \tfrac{1}{2}Fe_2O_3.$$

Excess Fe_2O_3 was used to ensure that enough subsurface oxygen was present to fully oxidise titanium and to allow easy reaction monitoring by CEMS since the outermost CEMS peaks of Fe_2O_3 are at positions easily distinguished from paramagnetic and magnetically relaxed components found near 0 mm s^{-1}.

First, ^{57}Fe (67.9% enriched, Oak Ridge National Laboratory) was evaporated onto precleaned 3.81 cm diameter quartz disks in a high-vacuum evaporator operated at a base pressure of 10^{-8} Pa. The evaporator was equipped with two independent 3 kW, three-crucible electron beam guns. A calibrated Inficon XTC crystal monitor and a pneumatic shutter assembly were used to control evaporation rates to 0.1 nm s^{-1} and to measure/control film thicknesses. Specimens were then transferred to an evacuated UHV compatible quartz reactor vessel (10^{-8} Pa) by a high-vacuum sample transporter (10^{-6} Pa) and heated to 773 K in 6.7 kPa of oxygen for 1 h to form Fe_2O_3. After transfer

back to the evaporator, FeTi was applied by alternating evaporations of 1.0 nm layers of titanium (99.9+%, AESAR) and ^{57}Fe until the appropriate overall thickness had been obtained. Deposition in this manner results in a FeTi layer slightly rich in iron (60 at.%) but which provides a CEMS singlet at -0.14 mm s^{-1}, consistent with FeTi, and which appears homogeneous during SIMS depth profiles at low sputter-rates [7]. Evaporation of the palladium overlayer (99.9+%, AESAR) followed. CEMS analyses were performed after most deposition steps.

2.2. Sample treatment

Vacuum and hydrogen annealing procedures were performed in a quartz reactor vessel.

Vacuum annealing at 473, 523 and 573 K ($\pm$10 K) was performed on specimen 1, figure 1. Elevated temperatures were maintained for 1 h and then the specimen was cooled to room temperature and transferred to the CEMS chamber for analysis. Following CEMS analysis after the 573 K anneal, the specimen was analysed by XPS then returned to the reactor vessel and annealed in 101 kPa of H_2 ($[H_2]/[H_2O] \approx 10^6$) for 1 h before being analysed again by CEMS.

Hydrogen annealing was also performed on specimen 2, figure 1. After the transfer of the specimen to the evacuated reactor vessel, H_2 gas was admitted up to a total pressure of 101 kPa. The temperature was then elevated and maintained at either 473, 523, 573, 623 or 673 K for 1 h. After annealing at each temperature, the specimen was allowed to cool in the H_2 gas environment before evacuation of the reactor and subsequent transfer to the CEMS chamber for analysis. XPS analysis was also performed after hydrogen annealing at 673 K. Specimens were stored in vacuum at all times except during hydrogen annealing treatments.

2.3. Sample analysis

CEMS allows the non-destructive monitoring of chemical, electronic and magnetic properties of subsurface components containing ^{57}Fe within the topmost 300 nm of the surface. All CEMS data were collected in an UHV chamber equipped with seven spiraltron electron multipliers operated at $\approx 10^{-8}$ Pa. Seven spectra were obtained simultaneously in the constant acceleration mode and these were summed to increase the effective counting rates. A 200 mCi ^{57}Co/Pd source was used with the positive velocity defined as the source approaching the absorber, and zero velocity referenced to the centroid of a metallic iron spectrum. All spectra were obtained at room temperature. Further details of the CEMS apparatus and data fitting routine have been described elsewhere [10].

XPS spectra were collected to obtain chemical state and quantitative information within the topmost 3 nm of the specimens. Data were obtained using a Leybold–Heraeus LHS-10 system operated at a based pressure of $\approx 10^{-8}$ Pa. An aluminium anode was used, and lattice oxygen, within the specimen at a binding energy of 531.0 eV, was used to calibrate the work function of the analyser. Fe/Pd atomic ratios were calculated using standard techniques based on measured spectral areas, correction factors for spectrometer efficiency, available cross-sections and escape depths.

3. Results

3.1. Vacuum annealing procedures

CEMS spectra for specimen 1 in figure 1 were collected after various preparation steps and after each vacuum annealing treatment as shown in figure 2.

3.1.1. Sample preparation. The spectrum obtained after preparation of the iron oxide layer is dominated by a Fe_2O_3 sextuplet having a hyperfine field of 516 KOe and an isomer shift of 0.42 mm s^{-1}. The fitted parameters match closely with values reported in the literature [11]. This sextuplet contains 94% of the total spectral area. An Fe^{3+} doublet with an isomer shift of 0.46 mm s^{-1} and a quadrupole splitting of 1.07 mm s^{-1} contains the remaining 6% area.

Deposition of FeTi yields a spectrum with a peak at -0.14 mm s^{-1} superimposed over the Fe^{3+} components discussed above. The isomer shift of FeTi is consistent with other studies [12, 13]. The FeTi singlet comprises 43% of the total spectral area and the Fe^{3+} components now comprise 57% of the total spectral area.

Addition of the palladium coating results in a change in the spectral area distribution of 38% and 62% for the FeTi and Fe^{3+} components, respectively. This effect results from the attenuation of resonant low-energy electrons (less than 50 eV) associated with surface ^{57}Fe by the palladium coating [14].

3.1.2. Vacuum annealing. A significant chemical reduction of Fe_2O_3 is noted after annealing at 473 K. Forty per cent of the total spectral area is contained in two sextuplets associated with Fe_3O_4 [11]. These sextuplets have hyperfine fields of 494 and 461 kOe and isomer shifts of 0.45 and 0.70 mm s^{-1}, respectively. Fe_2O_3 and FeTi have relative areas of 31 and 29%, respectively.

All hematite has been removed in the spectrum obtained after annealing at 523 K. To fit this spectrum it was necessary to include a broad, FWHM = 7 mm s^{-1}, component centred at 0 mm s^{-1}. This component has a relative area of 44% and can account for a number of iron phases including magnetically relaxed metallic iron, iron oxides and Fe–Pd alloys, as well as paramagnetic Fe–Ti and Fe–Pd alloys (Fe–Pd alloys containing less than 15% Fe [15, 16]). Relaxation of magnetically split components is known to occur for decreased domain sizes since they have an increased number of atoms at the domain interface which can experience anisotropic effects [17]. The relative areas of Fe_3O_4 and FeTi comprise 51 and 5% of the total spectral area, respectively.

Annealing the specimen to 573 K results in a spectrum that contains a component associated with an Fe–Pd alloy. This component was fitted using a sextuplet with a hyperfine field of 268 kOe and an isomer shift of 0.33 mm s^{-1}. The relative area is 25% of the total spectral area. The relative area of Fe_3O_4 comprises 74% of the total spectral area and FeTi is no longer detected.

A comparison to spectra obtained by Longworth [18] supports an assignment of the Fe–Pd alloy to either disordered $Fe_{0.22}Pd_{0.78}$ or ordered $Fe_{0.50}Pd_{0.50}$. To discern the appropriate assignment it was necessary to perform a material balance based on: (i) the original elemental content of the specimen, (ii) the CEMS relative area of 25%, and (iii) the bulk density values of iron and palladium. Such a procedure provides a maximum possible Pd/Fe atomic ratio of 2.2. Therefore, since there is insufficient palladium to form $Fe_{0.22}Pd_{0.78}$ (Pd/Fe = 3.5), the component must be assigned to ordered $Fe_{0.50}Pd_{0.50}$ and excess palladium.

XPS analysis of the Pd $3d_{3/2-5/2}$ and Fe $2p_{1/2-3/2}$ regions yielded a Pd/Fe ratio of 3.8 at the surface. Both iron and palladium were present in the zero-valent state and no titanium was observed on the surface. From a consideration of both XPS and CEMS data, it is evident that Fe–Pd alloying is in-homogeneous throughout the overall thickness of the specimen, and that the most extensive alloying has occurred at the buried Pd–Fe interface.

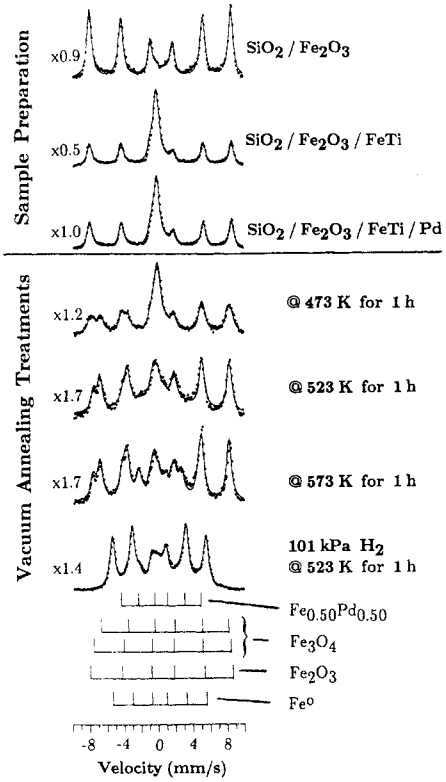

Figure 2. CEMS spectra for specimen 1, figure 1, after the indicated specimen preparation steps and vacuum annealing treatments.

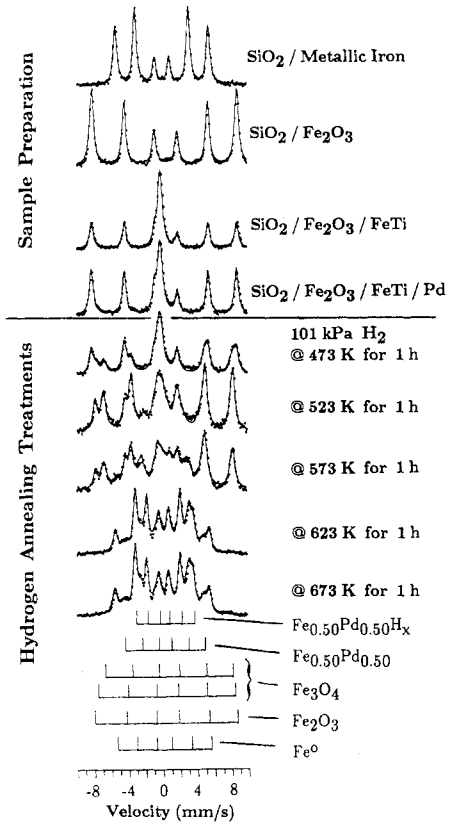

Figure 3. CEMS spectra for specimen 2, figure 1, after the indicated specimen preparation steps and hydrogen annealing treatments.

Almost complete reduction of Fe_3O_4 was observed in the spectrum obtained after performing a hydrogen annealing procedure at 523 K on the above noted specimen. A metallic-iron sextuplet having a hyperfine field of 330 kOe and an isomer shift of 0 mm s^{-1} constitutes 69% of the spectral area. About 6% of the spectral area is associated with an Fe^{2+} doublet having a quadrupole splitting of 2.00 mm s^{-1} and an isomer shift of 0.99 mm s^{-1}. The remaining 25% of the spectral area remains in the sextuplet associated with $Fe_{0.50}Pd_{0.50}$.

3.2. Hydrogen annealing procedures

The CEMS spectra for specimen 2 in figure 1 collected after various preparative steps and after each hydrogen annealing treatment are shown in figure 3.

3.2.1. Sample preparation. The spectrum obtained after iron deposition is comprised of a metallic iron sextuplet with a hyperfine field of 330 kOe and an isomer shift of 0 mm s^{-1}. Oxidation produces a similar spectrum as encountered in the Vacuum annealing spectrum discussed above. An Fe_2O_3 sextuplet is observed having a hyperfine field of 516 kOe and an isomer shift of 0.45 mm s^{-1}.

The addition of FeTi produces a spectrum comprised of an FeTi singlet at -0.14 mm s^{-1} imposed on the Fe_2O_3 sextuplet. The singlet and the sextuplet have relative areas of 43 and 57% of the total spectral area, respectively.

The palladium coating alters the relative areas of the components in a similar fashion as noted earlier. Hematite has a relative area of 69% while FeTi comprises 31% of the total spectral area.

3.2.2. Hydrogen annealing. As found for the corresponding vacuum annealing treatment, 101 kPa of H_2 gas at 473 K converts a large portion of Fe_2O_3 to Fe_3O_4. The relative areas of Fe_2O_3, FeTi and Fe_3O_4 are 36, 25 and 39%, respectively.

At a temperature of 523 K in H_2, all the Fe_2O_3 has been removed. Fe_3O_4 comprises 72% of the total spectral area while FeTi has essentially been removed. The remaining 25% of the spectral area was fitted to: (i) a sextuplet (17%) having a hyperfine field of 226 kOe and an isomer shift of 0.33 mm s^{-1} and (ii) a singlet (8%) at 0.20 mm s^{-1}. Both of these latter two components can be attributed to small domains of $Fe_{0.50}Pd_{0.50}$, some of which undergo magnetic relaxation [17].

The hydrogen annealing treatment at 573 K yields a complex spectrum. The relative area of Fe_3O_4 decreases to 49%. Fe^{2+} and Fe^{3+} doublets each contain 6% of the total spectral area with a metallic-iron sextuplet comprising 9% of the area. The metallic-iron sextuplet has a hyperfine field of 309 kOe, providing evidence for small particles having a characteristic dimension of 3.8 nm (cube root of the domain volume of 54 nm^3). The Fe–Pd alloy increases in relative area to 30% and experiences an increase in hyperfine field to 262 kOe. This hyperfine field is close to the bulk value of 267.9 kOe reported by Longworth [18] for ordered $Fe_{0.50}Pd_{0.50}$.

An increase in the H_2 annealing temperature to 623 K provides evidence for the formation of Fe–Pd hydrides. Côrrea *et al* [19, 20] show that for the ternary hydride Pd_3FeH_x, the magnetic hyperfine field in the hydride is approximately 30% smaller than the one observed for ordered Pd_3Fe. The data presented in figure 3 has a sextuplet component with a hyperfine field of 190 kOe that corresponds to a 28% decrease of the 263 kOe hyperfine field associated with the Fe–Pd alloy. Sextuplets for the hydrided and unhydrided alloys comprise 46 and 21%, respectively, of the total spectral area. The metallic-iron spectral area increases to 30% and the hyperfine field at 329 kOe is near that expected for bulk metallic-iron (i.e. 330 kOe).

The preparation of bulk Fe–Pd hydrides is often performed by electrolysis because preparation by hydrogen diffusion from the gas phase requires pressures of the order of 10^6 kPa [21]. Additionally, it has been shown by Côrrea *et al* [20] that near room temperature at atmospheric pressures, bulk hydrides begin to decompose. The rationale for obtaining Fe–Pd hydrides at conditions used in this study are as follows. First, the specimen in this study has small domains of Fe–Pd alloys near the surface so that high pressures, which are necessary for diffusion of hydrogen into the bulk, are not required. Second, since the specimen was cooled to room temperature in the presence of hydrogen, it is reasonable to expect that the hydride phase does not entirely decompose.

The final hydrogen anneal was performed at 673 K. The sextuplet associated with Fe–Pd hydrides has a hyperfine field of 190 kOe and accounts for 47% of the total spectral area. The Fe–Pd alloy yields a sextuplet with a hyperfine field of 268 kOe which is near that of bulk $Fe_{0.50}Pd_{0.50}$. This sextuplet has a relative area of 18%. A material balance using the original elemental content of the specimen, the CEMS areas, and the iron and palladium bulk densities yields a maximum possible Pd/Fe ratio of 0.9 which is near the ratio of 1.0 determined by XPS in the surface region. Agreement between these

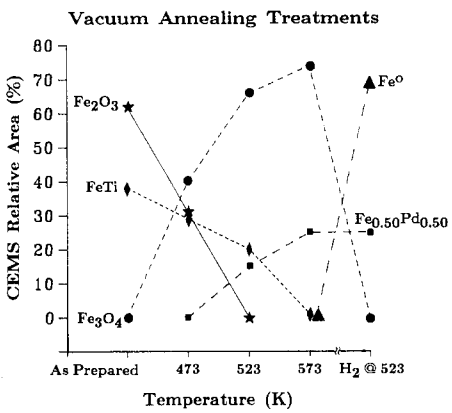

Figure 4. Plot of the CEMS relative areas versus vacuum annealing temperatures for components detected in the spectra shown in figure 2.

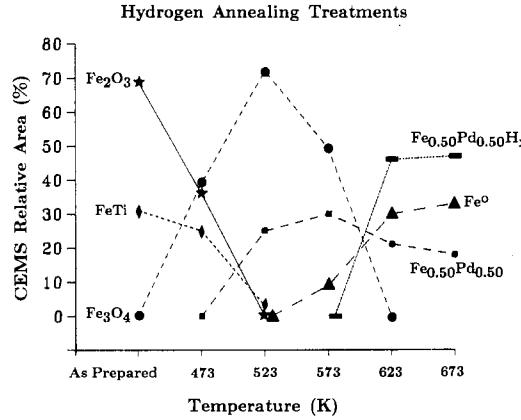

Figure 5. Plot of the CEMS relative areas versus hydrogen annealing temperatures for components detected in the spectra shown in figure 3.

techniques suggests that the alloyed region of the specimen is now nearly homogeneous throughout the film. The metallic-iron sextuplet retains a hyperfine field of 330 kOe with a relative area of 33%.

4. Discussion

Figures 4 and 5 show plots of the CEMS detected components during vacuum and hydrogen annealing procedures. The broad baseline obtained after the 523 K vacuum anneal (i.e. 44% of the relative area) was divided equally amongst the spectral areas reported for Fe_2O_3, FeTi and Fe–Pd as a result of the difficulty in deconvolution near zero velocity and the previously noted relation effects.

4.1. Annealing at temperatures ≤523 K

Vacuum and hydrogen annealing provide similar trends at temperatures up to 523 K. Fe_2O_3 is reduced to Fe_3O_4 at the expense of the FeTi layer. The formation of Fe–Pd alloys with an estimated composition of $Fe_{0.50}Pd_{0.50}$ also takes place. A material balance using hydrogen anneal data was performed to determine the Ti/O atomic ratio after the 523 K anneal. This procedure assumed that a closed system was provided by a contiguous palladium barrier and was based on CEMS spectral areas of all iron-containing components before hydrogen annealing (i.e. as fabricated) and after hydrogen annealing at 523 K. The material balance revealed that titanium and oxygen, originally contained in iron compounds, now exist as non-iron containing products with a Ti/O atomic ratio of 3.7. This ratio indicates that titanium has not been fully oxidised to TiO_2.

Known thermodynamic values for iron and titanium oxides provide justification for the transformations observed in figures 4 and 5. The Gibbs free energies of formation for Fe_3O_4, Fe_2O_3, TiO and TiO_2 at 298 K are: −253.9, −247.4, −495.0 and −444.8 kJ (mol O)$^{-1}$, respectively [22]. At 523 K, titanium at the Fe_2O_3/FeTi interface reacts with adjacent oxygen to form TiO or TiO_2 while Fe^{3+} in the Fe_2O_3 layer is reduced to form

the slightly more stable Fe_3O_4 compound. The similarity in the data at 523 K, and the apparent dependence of the reaction pathways on the stability/accommodation of oxygen, suggests that the palladium overlayer forms a contiguous barrier to oxygen-containing species at these conditions.

4.2. Annealing at temperatures ≥573 K

There is a noticeable difference in the plots for vacuum and hydrogen annealing procedures at 573 K. The vacuum annealing plot (figure 4) shows a continued increase in the Fe_3O_4 contribution from 523 K to 573 K. However, the hydrogen annealing plots at these same temperatures show a large decrease in Fe_3O_4 with the simultaneous formation of metallic iron. For the hydrogen anneal data, a material balance performed as discussed above yields a Ti/O ratio of 1.3 and supports a concurrent oxidation of titanium in FeTi as Fe_3O_4 is reduced. At 573 K, there are two possible driving forces for the reduction of Fe_3O_4 to iron metal. Iron oxides in the presence/contact of hydrogen are known to be easily reduced at $(H_2O)/(H_2)$ ratios less than 0.05 [23], and the oxidation of titanium is strongly preferred over iron oxides as noted by their relative Gibbs free energies.

For the 573 K vacuum annealing procedure, however, a material balance reveals that insufficient oxygen is present in the as-prepared specimen to account for all the Fe_3O_4 observed. Also, additional oxygen would be needed to form any titanium oxide components produced from the break-up of FeTi. This information suggests the formation of cracks or grain boundaries in the palladium overlayer allowing background impurities to permeate the overlayer and react with subsurface components.

The hydrogen annealing treatment, performed on specimen 1 after completion of all vacuum annealing treatments, substantiates the cracking hypothesis established above. Figure 4 shows that all the Fe_3O_4 is reduced to metallic iron. Apparently, the H_2 gas can readily contact subsurface Fe_3O_4 and cause complete reduction. These results are markedly different than those obtained for the hydrogen annealed specimen where complete reduction does not occur after hydrogen annealing at temperatures less than 623 K.

The increase in hyperfine field of the Fe–Pd alloy after hydrogen annealing at increasing temperatures reflects the growth in size of the hydride domains. Localised domains of approximately 22 nm^3 (determined from the measured hyperfine field of 226 kOe [17]) were formed at the Fe/Pd interface at 523 K. Continued alloying is reflected in larger domain sizes so that by 673 K, bulk hyperfine fields are observed. At this temperature, XPS results are in general agreement with an overall material balance, verifying the existence of a homogeneous Fe–Pd alloy surface layer with a composition near $Fe_{0.50}Pd_{0.50}$.

Thermodynamic considerations must also be given to the formation of alloys. Gibbs energies of formation for TiPd at 1873 K, FeTi at 1814 K and FePd at 1123 K have been determined to be −67, −20 and −18 kJ $(g\ atom)^{-1}$ [24, 25]. The greater stability of FeTi relative to FePd accounts for the unreactive nature of Pd/FeTi specimens which have been studied previously [8]. In this study, the higher stabilities of TiO and TiO_2 cause titanium to getter oxygen from iron oxides without the formation of Ti–Pd alloys. For the vacuum annealed specimen, oxygen is supplied by the reduction of Fe_2O_3 at temperatures ≤523 K; however, at temperatures ≥573 K, cracking allows titanium oxidation by background impurities as well. For the hydrogen annealed specimen, oxygen is supplied by the reduction of Fe_2O_3 at all temperatures. Thus, while FePd has

the largest Gibbs free energy, iron and palladium are the only free metals available for reaction.

Material balances, performed as discussed previously for the hydrogen annealed speciment at 523 K, were performed for the specimen after hydrogen annealing at 623 and 673 K. Both material balances yield Ti/O ratios of 0.3 which are sufficient to support complete oxidation of titanium to TiO_2 without additional oxygen from background impurities. Therefore, there is no reason to expect that the surface layer has become cracked as was determined for the vacuum annealed specimen at 573 K. One possible explanation for the stability of the palladium overlayer during hydrogen annealing is that the increase in lattice volume associated with FePd hydrogenation [26] is sufficient to minimise interfacial stresses that result from subsurface reactions.

5. Conclusions

The use of CEMS provides a means of investigating subsurface reactions with detail not obtainable by more conventional techniques. Compound identification can be established by unique fingerprints in the CEMS spectrum. Relative spectral areas provide quantitative information and allow the stoichiometry of reactions to be determined.

Investigation of Fe_2O_3/FeTi interfaces below palladium overlayers reveals significant differences between annealing in vacuum or in hydrogen. Vacuum annealing caused cracking of the palladium overlayer, allowing background impurities to oxidise subsurface titanium so that underlying iron oxides could not be significantly reduced by titanium in the FeTi layer.

Hydrogen annealing caused complete reduction of subsurface iron oxides at temperatures $\geqslant$623 K. Two driving forces are possible in this instance: (i) diffusion of hydrogen through the palladium overlayer, and (ii) titanium reactions with subsurface oxygen to produce titanium oxides and metallic iron.

This study suggests that palladium coatings can benefit FeTi hydrogen storage materials. A previous study of palladium overlayers on unoxidised FeTi verified coating compatibility and effectiveness as a barrier against O_2/H_2O impurities [8]. This study further demonstrates that deposition of thin palladium overlayers on oxidised surfaces can be used in the presence of hydrogen at elevated temperatures. Fe–Pd alloys have also been detected and apparently provide similar protection and hydrogen permeation as palladium.

Acknowledgments

We wish to acknowledge the Air Force Office of Scientific Research (AFOSR-84-G-0057) and the Army Research Office (DoD-URIP, DAAG28-84-0301) for financial support and appropriate equipment grants.

References

[1] Reilly J J and Wiswall R H 1974 *Inorg. Chem.* **13** 218
[2] Huston E L and Sandrock G D 1980 *J. Less-Common Met.* **74** 435
[3] Goodell P D, Sandrock G D and Huston E L 1980 *J. Less-Common Met.* **73** 135

[4] Dahiya R P (ed) 1987 *Progress in Hydrogen Energy* (Dordrecht: Reidel) p 84
[5] Schlapbach L and Riesterer T 1983 *Appl. Phys.* A **32** 169
[6] Sandrock G D and Goodell P D 1980 *J. Less-Common Met.* **73** 161
[7] Sanders J H and Tatarchuk B J 1989 *J. Less-Common Met.* **147** 277
[8] Sanders J H and Tatarchuk B J 1988 *J. Phys. F: Met. Phys.* **18** L267
[9] Khatamian D and Manchester F D 1985 *Surf. Sci.* **159** 381
[10] Zabinski J S and Tatarchuk B J 1988 *Nucl. Instrum. Methods Phys. Res.* B **31** 576
[11] Keisch B, Gibbon G A and Akhtar S 1977 *Fuel Processing Technol.* **1** 269
[12] Swartzendruber L J, Bennett L H and Watson R E 1976 *J. Phys. F: Met. Phys.* **6** L331
[13] Finkler D, Wagner H-G, Campbell S J, Blaes N and Gonser U 1985 *Z. Phys. Chem.* **145** 147
[14] Zabinski J S and Tatarchuk B J 1988 *Hyperfine Interact.* **41** 737
[15] Window B and Longworth G 1971 *J. Phys. F: Met. Phys.* **1** 718
[16] Oliver F W 1976 *J. Phys. Chem. Solids* **37** 1175
[17] Mørup S, Dumesic J A and Topsøe H 1980 *Applications of Mössbauer Spectroscopy* vol II, ed R L Cohen (New York: Academic) p 7
[18] Longworth G 1968 *Phys. Rev.* **172** 572
[19] Côrrea M H P, Vasquez A, Costa M I Jr, Viccaro P J and Gonçalves da Silva C E T 1981 *Solid State Commun.* **40** 211
[20] Côrrea M H P, Schreiner W H, Schmidt J E, Viccaro P J and Vasquez A 1985 *J. Phys. F: Met. Phys.* **15** 1779
[21] Flanagan T B, Majchrzak S and Baranowski B 1972 *Phil. Mag.* **25** 257
[22] Weast R C, Astle M J and Beyer W H (ed) 1984 *Handbook of Chemistry and Physics* ed R C Weast, 64th edn (Boca Raton, FL: Chemical Rubber Company) pp D70–D90
[23] Bohlbro H (ed) 1969 *An Investigation on the Kinetics of the Conversion of Carbon Monoxide with Water Vapour Over Iron Oxide Based Catalysts* (Copenhagen: Haldor Topsøe) p 164
[24] Choudary U V, Gingerich K A and Cornwell L R 1977 *Met. Trans.* A **8** 1487
[25] Alcock C B and Kubik A 1969 *Acta Metall.* **17** 437
[26] Carlow J S and Meads R E 1972 *J. Phys. F: Met. Phys.* **2** 982